PCB-Based Hybrid Series/Corporate-Fed 4×4 D-Band Phased Array with Wide-Angle Scanning

Kamil Yavuz Kapusuz, *Member, IEEE*, Samuel Rimbaut *Student Member, IEEE*, Siddhartha Sinha, *Member, IEEE* Joris Van Driessche, Ad C.F. Reniers, *Member, IEEE*, A.Bart Smolders, *Senior Member, IEEE*, Pascal Szriftgiser, Guillaume Ducournau, Hendrik Rogier, *Senior Member, IEEE*, and Sam Lemey, *Member, IEEE*

***Abstract*—A wideband 4×4 planar phased array, based on four hybrid series/corporate-fed 4×1 subarrays with an asymmetrically positioned wide-stripline stub, is proposed for next-generation D-band applications. Each subarray consists of a stripline power splitter and 180° phase shifter serving as a corporate feed for two co-optimized back-to-back series-fed arrays, each with two stripline-fed aperture-coupled stacked patch antennas. This hybrid feed approach minimizes the number of required feed layers, reducing both structural complexity and fabrication costs, while ensuring stable gain across a wide bandwidth. As a proof of concept, prototypes of a 4×1 subarray and a 4×4 array, with respective dimensions of 0.96×4.8 mm^2 and 3.8×4.8 mm^2, were fabricated using a standard any-layer high-density interconnect printed circuit board process for operation in the [120-150] GHz frequency band, demonstrating a 22% fractional bandwidth. The 4×1 and 4×4 arrays achieve peak gains of 10 dBi and 14.5 dBi, with total efficiencies of 58% and 55%, respectively, and support beam steering over ±45°. Furthermore, a 5 Gbaud 16-QAM wireless communication link over 26 cm distance was successfully established using the 4×4 array, achieving an error vector magnitude of less than 8%. This validates the use of the proposed antenna array at three carrier frequencies, enabling a 60 Gbit/s aggregated data rate for future multi-carrier D-band applications.**

***Index Terms*—Antenna array, D-band, hybrid series/corporate-fed, phased array, stacked patch antenna, subarray.**

I. Introduction

As fifth-generation (5G) deployment continues, sixth-generation (6G) networks aim to utilize the 100–300 GHz band to address the rising demands for high-capacity communication and fine-resolution sensing [1]. To overcome propagation challenges at these frequencies, future 6G systems will rely on highly directive phased arrays [2]. Combining massive multiple-input multiple-output (MIMO) with large bandwidths enables extreme throughput [3], but for commercialization, antenna systems must also be cost-effective, low-profile, and lightweight [4].

Recent advances in photolithography make printed circuit board (PCB)-based antenna arrays attractive beyond 100 GHz, offering low weight, cost efficiency, and IC integration [5]. Fully digital arrays provide flexibility [6]–[8] but face space, cost, and power constraints [9]. Subarray-based architectures provide more space for IC integration [10]. In particular, series-fed subarrays are simple and low-loss [11], but bandwidth is limited, while corporate-fed subarrays enhance bandwidth at the expense of footprint and efficiency [12]. Multilayer corporate feed implementation mitigates these drawbacks [13], though at higher complexity and cost. A combination of series and corporate feeding is essential to balance layer count, bandwidth, wide-angle scanning, feed-network losses, and IC integration. However, existing hybrid series/corporate-fed arrays operate at frequencies below 100 GHz [14]–[28] and lack simultaneous support of wide bandwidth, wide-angle scanning, and IC integration. This highlights the need for hybrid series/corporate-fed arrays that can achieve this balance at sub-THz frequencies, where optimizing the feed architecture to create room for IC integration, along with fabrication constraints, poses significant challenges.

This letter proposes a 4×4 planar antenna array, composed of four hybrid series/corporate-fed 4×1 subarrays, covering the [120-150] GHz band. Each subarray comprises a stripline power splitter and a 180° phase shifter, which together provide a corporate feed to two co-optimized, back-to-back (B2B) series-fed arrays, each featuring a pair of stripline-fed, aperture-coupled stacked patch antennas. This novel subarray topology introduces an asymmetric stub in its stripline feed to provide extra tuning parameters for wide-range coupling control beyond conventional no-stub or symmetric-stub designs, offering (i) a record-high bandwidth of 30 GHz, corresponding with a fractional bandwidth of 22%; (iii) only five metal layers, minimizing fabrication complexity; (iv) a compact footprint of $0.5\lambda_{\min}$ along the steering axis, making it an ideal building block to construct broadband arrays with a broad steering range, and (v) full compatibility with standard any-layer high-density interconnect (HDI) PCB technology [29], enabling cost-effective fabrication and seamless integration with beamforming ICs (BFICs).

In recent years, various PCB-based D-band arrays have been proposed to improve IC integration and bandwidth [see Table I]. Series-fed subarrays [30], [31] minimize layer count and allow IC integration, but their bandwidth is limited to below 5.7%. Corporate-fed arrays achieve up to 25% bandwidth [32], [33], yet their feed networks occupy the space needed for ICs and beam steering. Vertically-integrated feeds [13] mitigate this, but at the cost of high layer counts. Our proposed hybrid series/corporate-fed array surpasses current solutions in bandwidth and beam steering capability, maintaining a low, manageable layer count.

This research was funded by Ghent University under Grant BOF23/PDO/044 and BOF/STA/202109/043. Part of this work was funded by the French RENATECH network, the Equipex+ Nanofutur operated by the ANR, under the grant IA-21-ESRE-0012 and 2030 programs, CPER Wavetech and PEPR. The PEPR and Equipex+ Nanofutur are operated by ANR (grants ANR-22-PEEL-0006, ANR-22-PEFT-0006, and IA-21-ESRE-0012).

K.Y. Kapusuz, S. Rimbaut, H. Rogier, and S. Lemey are with IMEC and IDLab/EM Group, Ghent University, Ghent, Belgium.

S. Sinha and J. Van Driessche are with IMEC, Belgium.

A.C.F. Reniers and A.B. Smolders are with Eindhoven University of Technology, TU Eindhoven, Eindhoven 5612 AZ, Netherlands.

P. Szriftgiser is with Université de Lille, 59000 Lille, France.

G. Ducournau is with Université de Lille, CNRS, 59000 Lille, France.

TABLE I
PERFORMANCE OF STATE OF THE ART PCB-BASED D-BAND ARRAYS

Ref.	Size (mm^2)	AC	f_0 (GHz)	FBW (%)	Gain* (dBi)	SR (^{o})	NL
T.W.	**3.8×4.8**	**4×4**	**135**	**22**	**14.5**	**±45**	**5**
T.W.	**0.96×4.8**	**4×1**	**135**	**22**	**10**	**0**	**5**
[13]	8.8×8.8	8×8	148	15	17.4	±55	14
[30]	-	8×1	122	5.7	12.98	0	2
[31]	-	9×16	144	1.4	21	±40	2
[32]	4.3×4.3	4×4	145	14	14	0	4
[33]	6.5×6.5	4×4	140	25	17	0	5

f_0: Center frequency, AC: Array configuration, FBW: Fractional bandwidth, *Peak boresight gain, SR: Steering range, NL: Number of layers

II. HYBRID SERIES/CORPORATE-FED PHASED ARRAY

Fig. 1(a) depicts the architecture of the proposed linearly polarized planar phased array, designed for operation in the [120-150] GHz band. The array consists of four 4×1 subarrays, each with uniform element excitation, designed to achieve a stable gain exceeding 9 dBi and a return loss better than 10 dB across the full operating band. The footprint of each subarray must remain smaller than 1.1 mm × 5 mm ($0.55\lambda_{\text{min}} \times 2.5\lambda_{\text{min}}$, with λ_{min} the free-space wavelength at 150 GHz), to support grating-lobe-free beam steering within ±45° in the xz-plane. Moreover, the design must be compatible with standard any-layer-HDI PCB technology and ensure robustness against fabrication tolerances. Additionally, the array architecture should enable direct integration of the BFIC [34], [35] at its backside to minimize the overall system footprint and to reduce interference.

To meet these stringent design requirements, a hybrid series/corporate-fed aperture-coupled stacked-patch subarray topology with an asymmetrically positioned wide-stripline stub is proposed, as shown in Fig. 1(b). The proposed topology consists of four stacked patch antenna elements (metal layers M1 and M2), each fed by a stripline network (metal layers M3 to M5) through a rectangular coupling aperture. The stripline feed network, implemented across M3-M5, realizes the feeding scheme. First, elements AE1 and AE2 are combined into the first series-fed subarray, while AE3 and AE4 form the second. These two subarrays are fed by a stripline-based power splitter in metal layer M4 [see Fig. 1(b)], equally distributing the input signal to both series-fed subarrays [see Fig. 1(c)]. To ensure constructive radiation in the far-field, a 180° phase shift is applied by a transmission line between the output of the power splitter and the subarray composed of AE3 and AE4.

Each series-fed subarray contains a inner stacked patch (AE2, AE3) and an outer stacked patch antenna (AE1, AE4). The stand-alone inner stacked patch and end stacked patch antennas, each with identical dimensions, are first separately modeled in CST Studio Suite's full-wave frequency-domain simulator. Each antenna element provides a wide impedance bandwidth by carefully combining two resonances associated with the resonant patch lengths L_{u} and L_{b}. The bandwidth is influenced by the distance between the patches and the slot (h_1 and h_2), adjusted by selecting optimal substrate heights. A wide range of amplitude control is achieved through the stripline feed by introducing an asymmetrically positioned wide-stripline stub beneath each slot, as shown in Fig. 1(c). The parameter sweeps

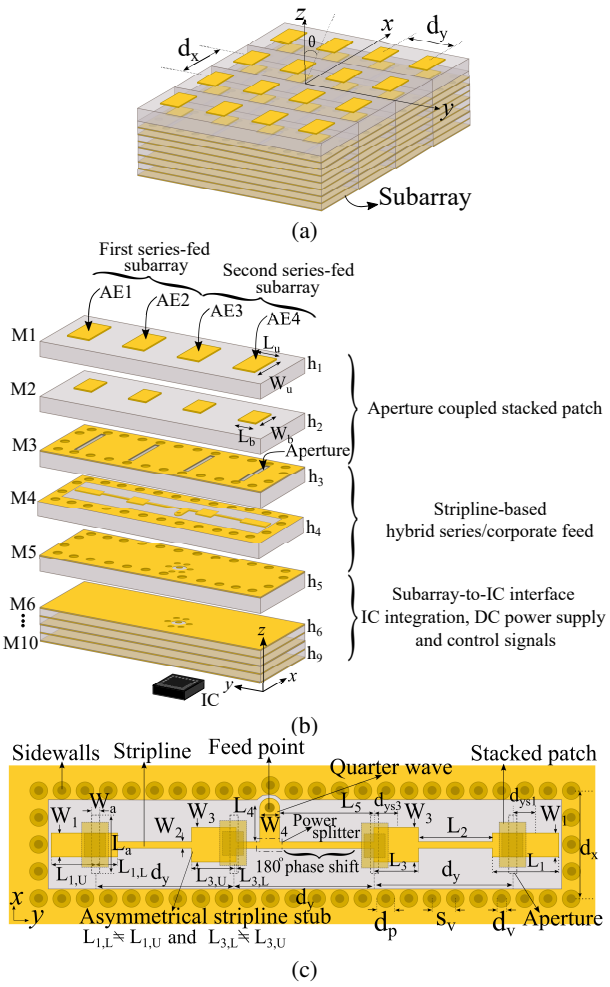

Fig. 1. (a) Concept and architecture of a planar phased array based on four-element subarrays. (b) Exploded view of the hybrid series/corporate-fed subarray. (c) Stripline-based subarray feed network, where both inner elements have the same dimensions and both outer elements have the same dimensions. Final dimensions: W_u = 690 μm, L_u = 460 μm, W_b = 380 μm, L_b = 360 μm, L_a = 500 μm, W_a = 60 μm, L_{1U} = 260 μm, L_{1L} = 68 μm, L_1 = L_{1L}+L_{1U}, d_{ys1} = 95 μm, L_2 = 660 μm, L_{3U} = 338 μm, L_{3L} = 18 μm, L_3 = L_{3L}+L_{3U}, d_{ys3} = 161 μm, L_4 = 240 μm, L_5 = 840 μm, W_1 = 210 μm, W_2 = 50 μm, W_3 = 300 μm, W_4 = 170 μm, d_v = 80 μm, s_v = 205 μm, d_p = 160 μm, d_x = 960 μm, d_y = 1240 μm, h_1 = 163 μm, h_2 = h_3 = 60 μm, h_4 = 65 μm.

in Fig. 2 demonstrate that a wide coupling range can be achieved. Specifically, in contrast to conventional no-stub or symmetric-stub designs, [30–70]% of the series feed input power can be coupled to the inner AE while the remainder is passed through to the outer element by jointly tuning the distance d_{ys3} and the stub dimensions W_3 and L_3. This enhanced tuning flexibility allows the array to be optimized for the required uniform amplitude excitation across all elements and a stable 40 Ω impedance across the targeted frequency band for each series-fed array, ensuring high array efficiency and stable radiation patterns. Two back-to-back series-fed arrays are then combined via a stripline power splitter, which incorporates a 180° phase shifter to ensure a broadside beam. The combined impedance is transformed to 50 Ω using a quarter-wave impedance transformer. To ensure constructive interference between the radiation of the inner and outer elements in the far field, the interconnecting line lengths between patches, d_{y}, is set to $0.55\lambda_0$, where λ_0 is

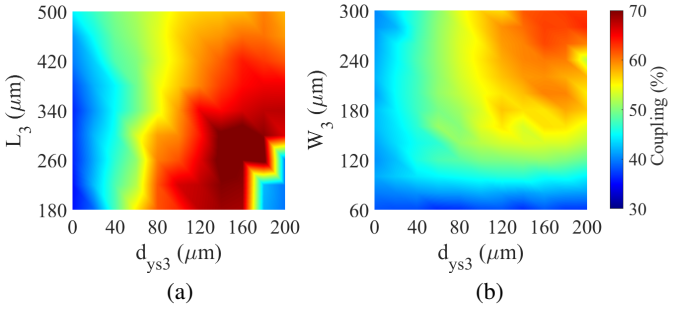

Fig. 2. Coupling to the inner radiating element with asymmetric stub [see Fig. 1(c)] as a function of (a) d_{ys3} and L_3 and (b) d_{ys3} and W_3, when W_2 = 65 μm.

the free-space wavelength at 135 GHz. This configuration achieves a narrow half-power beamwidth (HPBW) in the yz-plane of the four element subarray.

In the next step, a planar 4×4 array is designed based on the hybrid series/corporate-fed 4×1 subarray. It is composed of four 4×1 subarrays, totaling 16 antenna elements. The subarray spacing (d_x) of the array is set to approximately $0.5\lambda_{min}$ to ensure a grating-lobe-free scanning range exceeding ±45° in the horizontal (xz-) plane, as shown in Fig. 1(a). At this spacing, mutual coupling remains below –15 dB, guaranteeing stable performance over wide steering angles. The 4×4 array size is determined to be 3.84×4.76 mm² to accommodate 16 antenna elements, enabling direct interfacing to four transmit/receive chains [35].

III. Any-Layer HDI PCB Realization

The antenna (sub)arrays are fabricated using any-layer HDI PCB technology [36]. The antenna stackup comprises five 20 μm-thick metal layers (M1-M5) with a root-mean-square copper surface roughness profile of R_a = 300 nm [32] and four Panasonic Megtron 7 (ϵ_r = 3.2 and tan δ = 0.01) substrate layers, as shown in Fig. 1(b). Metal layers M5 to M10 are then included for digital, analog, and power supply signal routing to integrated ICs [34], [35]. Metal layer M5 serves as the bottom ground plane of the antenna, preventing undesired interaction between signal lines and the antenna layers. To achieve the target bandwidth, the thickness of substrate 1 is set to 163 μm thick, while substrates 2–9 are chosen to be thinner (60 μm and 75 μm-thick) to ensure acceptable transmission line widths and to implement laser-drilled stacked microvias.

Fig. 3(a) and Fig. 3(b) show photographs of the fabricated 4×1 subarray and 4×4 array prototypes, respectively. To characterize the performance of the 4×4 planar array, a grounded coplanar waveguide (GCPW) corporate feed with two stages of power splitters is realized on the PCB's back to excite the four subarrays. Yet, when a BFIC is integrated, this additional corporate feed network is not needed [34], [35].

IV. Measurement Results

A. S-Parameters and Radiation Performance

In this letter, backside probing is performed using a GSG-150-BT-N Picoprobe [37] and a Keysight N5227B Microwave Network Analyzer [38], coupled with Virginia Diode Incorporated (VDI)'s D-band VNA extenders [39] for both the reflection coefficient and far-field measurements. A thru–reflect–line

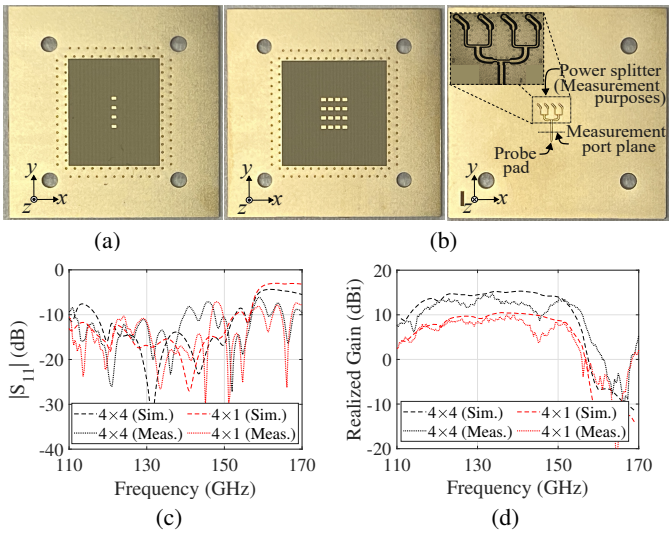

Fig. 3. Fabricated prototypes realized in PCB technology: (a) Top view of the 4×1 subarray and (b) top and back view of the 4×4 array. Measured and simulated (c) $|S_{11}|$ and (d) broadside gain over frequency.

calibration is performed to measure the S-parameters of the prototypes. Far-field radiation patterns are measured by the gain comparison method using a standard gain horn [40].

The measured reflection coefficients for both the 4×1 subarray and the 4×4 array, shown in Fig. 3(c), indicate a -8 dB impedance bandwidth spanning from 120 GHz to 155 GHz, yielding a 35 GHz bandwidth for both configurations. Notably, for the 4×1 subarray around 147 GHz, the reflection coefficient only reaches -8 dB within a 3 GHz range whereas the measured matching is reduced to -8.5 dB around 141 GHz and 146 GHz for the 4×4 array. Aside from these narrow regions, both prototypes achieve full coverage of the [120–150] GHz band with a reflection coefficient magnitude below -10 dB.

In Fig. 3(d), the simulated and measured maximum gains across the operating band show good agreement, with measured peak realized gains 10 dBi for the subarray and 14.5 dBi for the 4×4 array, establishing them as strong candidates for D-band applications. Around 145 GHz, the measured gain drops more than simulated. While increased impedance mismatch contributes to this, its severity and narrowband nature suggests that an unintended resonance or interaction in the measurement setup may also be affecting the gain.

Fig. 3 illustrates good agreement between the simulated and measured radiation patterns (co- and cross-polarization) at 135 GHz. The difference in maximum gain between the simulation and measurement equals 0.5 dB for the 4×4 array. Moreover, the measured cross-polarization ratio consistently remains above 35 dB. Uncertainty in measurements arises from the absorbers surrounding the antenna-under-test, which are used to cover the antenna carrier [41]. For the 4×1 subarray, a total efficiency of 58% is observed at 135 GHz. Based on the associated full-wave simulation model, this efficiency reduction can mainly be attributed to dielectric losses (27%), followed by conductor and surface roughness loss (8%), and mismatch loss (7%). Similar observations apply to the full 4×4 array, which exhibits a measured efficiency of 55% at 135 GHz.

The measured and simulated radiation patterns of the

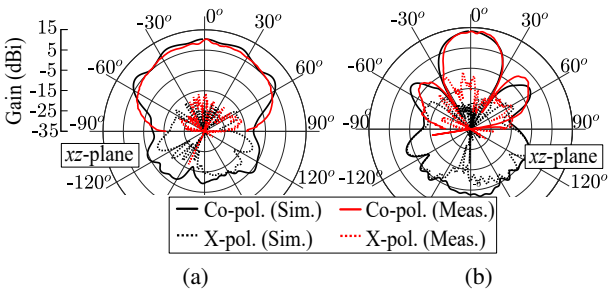

Fig. 4. Simulated and measured co-polarized and cross-polarized radiation patterns at 135 GHz of the (a) 4×1 subarray and (b) 4×4 array.

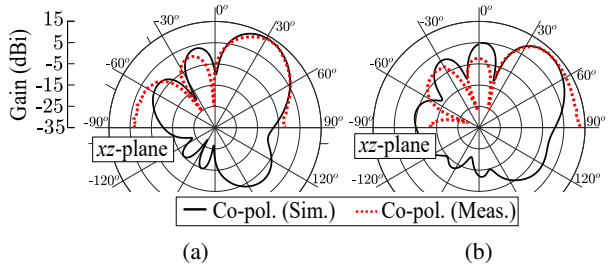

Fig. 5. Simulated and measured co-polarized radiation pattern of 4×4 antenna array at 135 GHz steered to (a) θ = 30^o and (b) θ = 45^o.

subarray were postprocessed using uniform-amplitude phase-shifted excitations to demonstrate beam steering. While Fig. 5 illustrates representative cases at 30° and 45° for demonstration purposes, measurements were additionally performed across the entire –50° to 50° range. These results confirm fine-resolution and distortion-free steering, with the realized peak gain consistently lying within 13.5±1 dBi and without blindspots.

B. Over-the-Air (OTA) Measurements

1) Experimental setup: OTA data-link measurements were performed using the setup in Fig. 6(a). An optically modulated D-band signal was fed to the 4×4 array under test (AUT) through a high-speed photodiode [43] and a 100-μm-pitch GSG coplanar probe [44]. The AUT radiated downward, while a silver mirror redirected the signal to a WR6.5 horn antenna 260 mm away, which fed the captured signal to a D-band receiver. The receiver architecture and optical modulation were replicated based on [43]. A Mach–Zehnder modulator, driven by two baseband waveforms, generated the optical signal, which is then combined with a secondary laser via a fiber coupler to set the D-band frequency offset. At the receiver, a mixer [45] down-converted the D-band signal to an intermediate frequency (IF) below 40 GHz, with equalization applied to counter sub-harmonic mixer (SHM)-induced roll-off. The SHM local oscillator (LO), operating at half the RF, was derived from a sixfold-multiplied SMA100B source. The amplified IF was analyzed in real time using a Keysight UXR0704AP oscilloscope, and linear equalization in VSA software [46] compensated for frequency-dependent losses, IF amplification, and cable effects.

2) Results: Based on the measured broadside antenna gain [Fig. 3(b)], 3 carriers were defined: 125 GHz, 135 GHz and 149 GHz, where the gain remains stable to minimize signal distortion. Transmission power was controlled by adjusting the optical power coupled to the photodiode. The initial performance was characterized in a B2B configuration, where the transmit and receive reference planes [Fig. 6(a)] were directly connected and the magnitude of the error vector (EVM) was measured as a function of the received power. The wireless link was then evaluated under identical conditions, with EVM recorded across the same channels. Fig. 6(b) shows the measured spectra of the AUT across these 3 channels, each normalized to its maximum, with a 5-GBaud 16-QAM signal transmitted per channel.

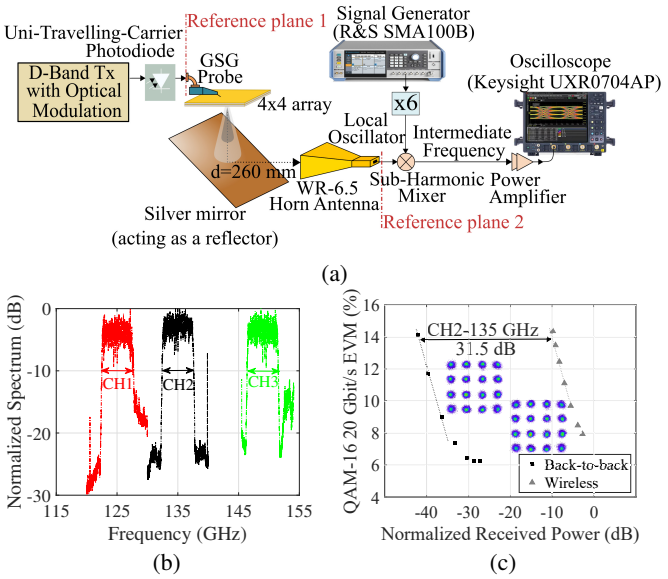

Fig. 6. (a) Block diagram of the over-the-air measurement setup. (b) Normalized signal spectrum received by oscilloscope. (c) EVM performance and output constellation for both the experimental setup and back-to-back configuration over a 260-mm link.

Fig. 6(c) displays the demodulated constellations at 135 GHz, where the measured power penalty with respect to the B2B configuration equals 31.5 dB, closely aligning with the -32 dB $|S_{21}|$ value obtained during antenna testing. This similar transmission trend confirms the antenna's suitability as a Tx antenna for the system. The other two channels were also tested, revealing that the wireless performance exhibits a similar trend, with measured power penalties of 34 dB at both 125 GHz and 149 GHz, again closely aligning with measured $|S_{21}|$-values -33 dB and -34 dB, respectively. These findings validate the performance of the proposed antenna array across the target frequency band and demonstrate the support of an aggregated data rate of 60 Gbit/s, an output that can be effectively managed by the array in conjunction with future multi-carrier D-band transmitters.

V. Conclusion

A novel wideband 4×4 antenna array, built from four hybrid series/corporate-fed 4×1 subarrays, is proposed for D-band applications. The feed network, with asymmetrical stripline stub, reduces layer count and structural complexity while maintaining stable, wideband gain. Measurements of the 4×4 array and a 4×1 subarray show efficiencies over 58% and 55%, peak boresight gains of 14 dBi and 10 dBi, and a bandwidth covering [120-150] GHz. The 4×4 array also supports ±45^o scanning, validating its suitability for wideband beamsteering and enabling an aggregated 60 Gbit/s data rate with a multi-carrier D-band transmitter.

REFERENCES

[1] A. Kaushik *et al.*, "Toward integrated sensing and communications for 6G: Key enabling technologies, standardization, and challenges," *IEEE Commun. Stds. Mag.,* vol. 8, no. 2, pp. 52–59, June 2024.

[2] T.S. Rappaport *et al.*, "Wireless communications and applications above 100 GHz: Opportunities and challenges for 6G and beyond," *IEEE Access,* vol. 7, pp. 78729-78757, 2019.

[3] A. Karakuzulu, M.H. Eissa, D. Kissinger, and A. Malignaggi, "A four-channel bidirectional D-band phased-array transceiver for 200 Gb/s 6G wireless communications in a 130-nm BiCMOS technology," *IEEE J. Solid-State Circuits*, vol. 58, no. 5, pp. 1310-1322, May 2023.

[4] M.J.W. Rodwell, A.S.H. Ahmed, M. Seo, U. Soylu, A. Alizadeh, and N. Hosseinzadeh, "IC and array technologies for 100-300 GHz wireless," *in Proc. IEEE Custom Integr. Circuits Conf.*, Apr. 2022, Newport Beach, CA, USA, pp. 1-5.

[5] M. De Kok, A.B. Smolders, and U. Johannsen, "A review of design and integration technologies for D-band antennas," *IEEE Open J. Antennas Propag.*, vol. 2, pp. 746-758, 2021.

[6] A. Ahmed, L. Li, M. Jung, S. Li, D. Baltimas, and G.M. Rebeiz, "140-GHz 2-D scalable on-grid 8×8-element transmit–receive phased arrays with up/down converters demonstrating a 5.2-m link at 16 Gbps," *IEEE Trans. Microw. Theory Techn.*, vol. 72, no. 5, pp. 2852-2868, May 2024.

[7] H. Kim, J. Jung, W. Lee, S. Nam, and J. Oh, "D-band 4×4 multi-feed array antenna-in-package for high-power combining and polarization synthesis," *IEEE Access*, vol. 11, pp. 144006–144016, 2023.

[8] H. Kim and J. Oh, "140-GHz wideband array antenna-in-package using multimode resonance," *IEEE Trans. Antennas and Propag.*, vol. 71, no 3, pp. 2136–2144, March 2023.

[9] B. Sadhu, X. Gu, and A. Valdes-Garcia, "The more (antennas), the merrier: A survey of silicon-based mm-wave phased arrays using multi-IC scaling," *IEEE Microw. Mag.*, vol. 20, no. 12, pp. 32-50, Dec.2019.

[10] Y. Ertugrul, K.Y. Kapusuz, C. Desset, and S. Pollin, "Arbitrary subarrayed planar array antenna with sidelobe level control based on a Graph theory," *IEEE Antennas Wireless Propag. Lett.*, vol. 23, no 12, pp. 4198-4202, Dec. 2024.

[11] A.A. Farid, A.S.H. Ahmed, A. Dhananjay, and M.J.W. Rodwell, "A fully packaged 135-GHz multiuser MIMO transmitter array tile for wireless communications," *IEEE Trans. Microw. Theory Techn.*, vol. 70, no. 7, pp. 3396-3405, July 2022.

[12] Y.J. Cheng, Y.X. Gui, and Z.G. Liu, "W-band large-scale high-gain planar integrated antenna array," *IEEE Trans. Antennas Propag.*, vol. 62, no. 6, pp. 3370–3373, Jun. 2014.

[13] D. Jung *et al.*, "Terahertz antenna-in-package design and measurement for 6G communication systems," *IEEE Trans. Antennas and Propag.*, vol. 72, no. 2, pp. 1085-1096, Feb. 2024.

[14] H.D. Li and L. Zhu, "Horizontally polarized array antenna using hybrid resonant mode for millimeter-wave wadar application," *IEEE Antennas Wireless Propag. Lett.*, vol. 23, no. 9, pp. 2802-2806, 2024.

[15] Z. Li, S. Gao, L. Chang, and Y. Li, "Compact and single-fed cavity-cascaded antenna array with horizontal polarization based on microstrip line," *IEEE Trans. Antennas Propag.*, vol. 72, no. 10, pp. 8040-8045, 2024.

[16] Q. Chen *et al.*, "A low sidelobe 77 GHz centre-fed microstrip patch array antenna," *IET Microw., Antennas & Propag.*, vol. 17, no. 11, pp. 887-896, 2023.

[17] B. Wang, Z. Zhao, K. Sun, C. Du, X. Yang, and D. Yang, "Wideband series-fed microstrip patch antenna array with flat gain based on magnetic current feeding technology," *IEEE Antennas Wireless Propag. Lett.*, vol. 22, no. 4, pp. 834-838, 2023.

[18] N. Kalva and B.M. Kumar, "Feedline design for a series-fed binomial microstrip antenna array with no sidelobes," *IEEE Antennas Wireless Propag. Lett.*, vol. 22, no. 3, pp. 650–654, 2023.

[19] H. Aliakbari, M. Mosalanejad, C. Soens, G.A.E. Vandenbosch, and B.K. Lau, "79 GHz multilayer series-fed patch antenna array with stacked micro-via loading," *IEEE Antennas Wireless Propag. Lett.*, vol. 21, no. 10, pp. 1990–1994, 2022.

[20] S. Yoo, Y. Milyakh, H. Kim, C. Hong, and H. Choo, "Patch array antenna using a dual coupled feeding structure for 79 GHz automotive radar applications," *IEEE Antennas Wireless Propag. Lett.*, vol. 19, no. 4, pp. 676-679, 2020.

[21] G. Sacco, P. D'Atanasio, and S. Pisa, "A wideband and low-sidelobe series-fed patch array at 5.8 GHz for radar applications," *IEEE Antennas Wireless Propag. Lett.*, vol. 19, no. 1, pp. 9–13, 2020.

[22] R. Chopra and G. Kumar, "Series-fed binomial microstrip arrays for extremely low sidelobe level," *IEEE Trans. Antennas Propag.*, vol. 67, no. 6, pp. 4275–4279, 2019.

[23] H. Chu, P. Li, X.-H. Zhu, H. Hong, and Y. Guo, "Bandwidth improvement of center-fed series antenna array targeting for base stations in offshore 5G communications," *IEEE Access,* vol. 7, pp. 33537-33543, 2019.

[24] H. Khalili, K. Mohammadpour-Aghdam, S. Alamdar, and M. Mohammad-Taheri, "Low-cost series-fed microstrip antenna arrays with extremely low sidelobe levels," *IEEE Trans. Antennas Propag.*, vol. 66, no. 9, pp. 4606-4612, 2018.

[25] Y.Q. Guo, Y.M. Pan, and S.Y. Zheng, "Design of series-fed, single-layer, and wideband millimeter-wave microstrip arrays," *IEEE Trans. Antennas Propag.*, vol. 68, no. 10, pp. 7017-7026, 2020.

[26] M. Mosalanejad, I. Ocket, C. Soens, and G.A.E. Vandenbosch, "Wideband compact comb-line antenna array for 79 GHz automotive radar applications," *IEEE Antennas Wireless Propag. Lett.*, vol. 17, no. 9, pp. 1580-1583, 2018.

[27] L. Chang, Z. Zhang, Y. Li, and Z. Feng, "All-metal antenna array based on microstrip line structure," *IEEE Trans. Antennas Propag.*, vol. 64, no. 1, pp. 351-355, 2016.

[28] K. Wincza and S. Gruszczynski, "Microstrip antenna arrays fed by a series-parallel slot-coupled feeding network," *IEEE Antennas Wireless Propag. Lett.*, vol. 10, pp. 991-994, 2011.

[29] "IPC International, inc. sectional design standard for high density interconnect (HDI) printed boards," 2024, accessed on June 7, 2024. [Online]. Available: https://www.ipc.org/TOC/IPC-2226A.pdf

[30] R. Hasan, W.A. Ahmed, J.-H. Lu, H.J. Ng, and D. Kissinger, "F-band differential microstrip patch antenna array and waveguide to differential microstrip line transition for FMCW radar sensor," *IEEE Sensors J.*, vol. 19, no. 15, pp. 6486–6496, Aug. 2019.

[31] S. Abu-Surra *et al.*, "End-to-end 140 GHz wireless link demonstration with fully-digital beamformed system," *in Proc. IEEE Int. Conf. on Commun. Workshops*, 2021, Montreal, QC, Canada, pp. 1-6.

[32] A. Lamminen, J. Säily, J. Ala-Laurinaho, J. de Cos, and V. Ermolov, "Patch antenna and antenna array on multilayer high-frequency PCB for D-band," *IEEE Open J. of Antennas and Propag.*, vol. 1, pp. 396-403, 2020.

[33] T. Dao, A. Kearns, D.R. Paredes, and G. Hueber, "Wideband high-gain stacked patch antenna array on standard PCB for D-band 6G communications," *IEEE Antennas Wireless Propag. Lett.*, vol. 23, no. 2, pp. 478-482, Feb. 2024.

[34] Y. Zhang *et al.*, "A 56Gb/s zero-IF D-band transmitter for a beamformer in 22nm FD-SOI," *in Proc. IEEE Radio Freq. Integr. Circuits Symp.*, Jun. 2024, Washington, DC, pp. 1-3.

[35] Y. Zhang *et al.*, "A 56Gbps zero-IF D-band transmitter in 22nm FD-SOI," *IEEE Trans. Microw. Theory Techn.*, under review.

[36] H. Aliakbari, M. Mosalanejad, C. Soens, G.A.E. Vandenbosch, and B.K. Lau, "Wideband SIW-based low-cost multilayer slot antenna array for E-band applications," *IEEE Trans. Compon., Packag., Manuf. Technol.*, vol. 9, no. 8, pp. 1568–1575, Aug. 2019.

[37] "SG-150-BT-N Picoprob," 2024, accessed on June 7, 2024. [Online]: https://ggb.com/wp-content/uploads/2017/06/mod170.pdf

[38] "N5227B PNA Microwave Network Analyzer," 2024, accessed on June 7, 2024. [Online]: https://www.keysight.com/us/en/product/N5227B/pna-microwave-network-analyzer-900-hz-10-mhz-67-ghz.html

[39] "Virginia Diode Incorporated website," 2024, accessed on June 7, 2024. [Online]: Available: https://www.vadiodes.com/en

[40] "The Flann Standard Gain Horns," 2024, accessed on June 7, 2024. [Online]: Available: https://flann.com/wp-content/uploads/2024/07/Series-240-Datasheet.pdf

[41] M. Verdaasdonk, A. Bart Smolders and A. C. F. Reniers, "Uncertainties introduced by the probe in millimeter-wave planar near-field measurements," *IEEE Trans. Antennas Propag.*, vol. 72, no. 6, pp. 4862-4873, June 2024.

[42] C. Balanis, Antenna Theory: Analysis and Design. Hoboken, NJ, USA: Wiley, 2005.

[43] H.N. Khelil *et al.*, "Aggregated 0.3 Tbit/s link using photonics-transmitter and micromachined flat array antenna over 315-410 GHz", *in Proc. Eur. Microw. Conf.*, Sept. 2024, Paris, France.

[44] "Cascade Infinity Waveguide Probe." [Online]. Available: https://www.formfactor.com/product/probes/infinity/infinity-waveguide-probe/.

[45] "Mixers-VDI Model: WR6.5 SHM." [Online]. Available: https://vadiodes.com/en/wr6-5shm.

[46] "PathWave Vector Signal Analysis." [Online]. Available: https://www.keysight.com/us/en/products/software/pathwave-test-software/89600-vsa-software.html